Engineering Structures 265 (2022) 114497

Contents lists available at ScienceDirect

Engineering Structures

journal homepage: www.elsevier.com/locate/engstruct

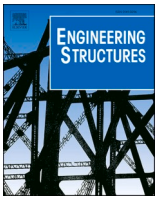

Seismic shear behavior of new high-strength reinforced concrete column and steel beam (New RCS) joints

Yu-Chen Ou [a,*], Nguyen Van Bao Nguyen [a,b], Wei-Ru Wang [a]

[a] Department of Civil Engineering, National Taiwan University, No. 1, Sec. 4, Roosevelt Road, Taipei 106, Republic of China
[b] Department of Civil Engineering, The University of Danang—University of Technology and Education, 48 Cao Thang Street, Danang 550000, Vietnam

ARTICLE INFO

Keywords:
RCS joint
High strength
Concentric
Eccentric
Shear strength

ABSTRACT

New high-strength reinforced concrete column and steel beam (New RCS) joints were developed in this research. Two-way, through-beam New RCS joint details with beams concentrically or eccentrically connected to the joint were proposed. The beam in one direction was continuous through the joint (continuous beam). The beam in the other direction was connected to the continuous beam by complete joint penetration (CJP) groove welds. Five-spiral reinforcement was used for joint transverse reinforcement. A method to calculate the amount of five-spiral reinforcement was proposed considering the confinement effect from the face-bearing plates (FBPs). Doubler plates were used to strengthen the eccentric beam flanges with predrilled holes to allow the passage of column longitudinal reinforcement. A method was proposed for the design of the doubler plates. Large-scale New RCS joint specimens designed to fail in joint shear were tested. Test results showed that the proposed joint details and design methods effectively avoided failure in undesirable locations. All the specimens failed in joint shear but still reached high drift ratios. The eccentric joint specimens (IDEHS and ISEHS) exhibited peak joint shears higher than the concentric beam specimen (IHS). The 1994 ASCE and 2015 ASCE shear strength models produced conservative predictions of the peak joint shear and the joint shear at 0.5% joint shear deformation for all the specimens. The predictions by the 2015 ASCE method were more reasonable with less scatter than the 1994 ASCE method because the former recognizes the shear strength contribution from the outer joint panel even without the use of shear keys and allows a longer steel web in shear strength calculation.

1. Introduction

Reinforced concrete column and steel beam (RCS) structures are a type of composite frame that effectively combines the advantages of reinforced concrete and steel. The cost of reinforced concrete columns is typically lower than comparable steel columns. This advantage becomes even more significant as the price of steel soars recently. On the other hand, for the same depth of the beam, steel beams typically can achieve a longer span than reinforced concrete beams. This allows for a building with fewer columns, particularly favorable for office use. As a result, RCS structures have gained more attention in Taiwan for office buildings.

In 1994, ASCE published guidelines for designing the beam-column joints of RCS frames for use in low-to-moderate seismic zones [1]. The guidelines resulted from several studies on the seismic behavior of RCS frames conducted in the 1980s and 90s [2,3]. In the guidelines, design methods for the through-beam type of joints of RCS frames were presented. These included methods for joint shear and bearing strength calculations and detailing considerations for transverse reinforcement within and adjacent to joints, face and extended face bearing plates, the size limit of column longitudinal bars, and others. Later, RCS frames' test results based on the ASCE guidelines [4–8] showed that the guidelines could also be used for regions of high seismicity. Moreover, design methods [9–12] were proposed to cover more joint details, and improved joint shear and bearing strength calculation methods were developed. Important new joint details included transverse beams and headed studs to mobilize joint shear strength contribution from the outer joint panel, and steel band plates to confine the column right above and below the joint. Important improvements for joint strength calculation included proper consideration of joint strength difference between interior and exterior joints, limiting the deformation of the joint for damage control, and treating the vertical bearing strength as the upper limit of the joint shear strength contribution from the inner joint panel. More recently, Alizadeh et al. [13] introduced additional bearing plates to increase the joint bearing strength. Mirghaderi et al. [14]

* Corresponding author.
E-mail address: yuchenou@ntu.edu.tw (Y.-C. Ou).

https://doi.org/10.1016/j.engstruct.2022.114497
Received 27 February 2022; Received in revised form 4 May 2022; Accepted 30 May 2022
Available online 9 June 2022

Nomenclature

A_c	concrete area confined by five-spiral reinforcement
A_{ch}	cross-sectional area enclosed by the outside edges of five-spiral reinforcement
A_g	gross area of concrete cross-section
A_h	cross-sectional loss of steel beam flange due to drilled holes
A_{hc}	concrete area confined by the FBPs and beam webs and flanges
A_{uc}	unconfined concrete area
b_f	width of steel beam flange
b_i	width of inner concrete panel
b_o	effective width of outer concrete panel
b_p	width of FBP
C	coefficient to account for the effect of stress concentration around the holes
C_{cn1}	nominal compression strength of bearing zone calculated by 1994 ASCE guidelines
C_{cn2}	nominal compression strength of bearing zone calculated by 2015 ASCE draft Pre-Standard
d_h	diameter of holes on steel beam flanges
d_j	effective joint depth determined as the distance between steel beam flange centerlines
d_w	depth of the beam web
$D_L^{'}$	outside diameter of large spiral
$D_S^{'}$	outside diameter of small spiral
$f_c^{'}$	specified compressive strength of concrete
$f_{ca}^{'}$	actual compressive strength of concrete
f_y	specified yield strength of reinforcement and steel plate SN490B
f_{ya}	actual yield strength of reinforcement and steel plate SN490B
f_{yt}	specified yield strength of transverse reinforcement
f_{ua}	actual ultimate strength of reinforcement and steel plate SN490B
F_{ysp}	yield strength of the steel beam web in the joint
h	height of the concrete column measured parallel to the beam
jh	horizontal distance between the resultant of the internal force couple
k_f	concrete strength factor
$M_{p,actual}$	nominal moment strength of the beam based on actual material properties
M_{test}	measured average maximum moment of the test beams at the column face
$\sum M_{test}$	total measured average maximum moment of the test beams at the column face
M_{vb1}	bearing moment strength of joint calculated by 1994 ASCE guidelines
M_{vb2}	bearing moment strength of joint calculated by 2015 ASCE draft Pre-Standard
P_u	axial force
t_r	thickness of doubler plate
t_{sp}	thickness of the steel beam web in the joint
V_b	bearing capacity between the beam flange and the column
V_{b1}	bearing capacity between the beam flange and the column predicted by ASCE guidelines 1994
V_{b2}	bearing capacity between the beam flange and the column predicted by ASCE draft Pre-Standard 2015
$V_{beam,test}$	applied load measured at the end of the test beam
V_{col}	measured column shear
V_{icn}	predicted inner diagonal concrete strut
V_{icn1}	inner diagonal concrete strut predicted by ASCE guidelines 1994
V_{icn2}	inner diagonal concrete strut predicted by ASCE draft Pre-Standard 2015
V_n	nominal joint shear strength
V_{n1}	nominal joint shear strength predicted by 1994 ASCE guidelines
V_{n2}	nominal joint shear strength predicted by 2015 ASCE draft Pre-Standard
V_{on}	predicted outer diagonal concrete strut
V_{on1}	outer diagonal concrete strut predicted by ASCE guidelines 1994
V_{on2}	outer diagonal concrete strut predicted by ASCE draft Pre-Standard 2015
V_{spn}	predicted horizontal shear strength of steel web panel
V_{spn1}	horizontal shear strength of steel web panel predicted by ASCE guidelines 1994
V_{spn2}	horizontal shear strength of steel web panel predicted by ASCE draft Pre-Standard 2015
V_{test}	measured average peak joint shear, $V_{test} = \frac{\sum M_{test}}{d_j} - V_{col}$
$V_{test\_0.5}$	measured joint shear corresponding to 0.5% joint shear deformation
α_{sp}	coefficient differentiating interior and exterior joints
α_c	strength factor depending connection type
β_1	stress block depth coefficient determined by 1994 ASCE guidelines
β_1^*	stress block depth coefficient determined by 2015 ASCE draft Pre-Standard
γ	reduction factor
γ_y	shear yield strain
ε_y	longitudinal yield strain
ρ_s	volumetric ratio of spirals
$\rho_{s,ACI}$	minimum amount of confinement reinforcement specified by ACI 318–19
$\rho_{s,prop}$	proposed amount of transverse reinforcement

proposed to place the through-beams outside the beam-column joint to eliminate the interference of through-beams with the column joint region. Eghbali and Mirghaderi [15] used vertical through-plates and shear connectors to transfer beam forces into the concrete column. Khaloo and Doost [16] welded steel channels to the face-bearing plates and to the through-beam flanges to increase the vertical and horizontal shear transfer, respectively. Lee et al. [17] investigated simplified connection details using face bearing plates, transverse beams, and shear studs to increase shear transfer across the joint. Test results showed the proposed simplified connection details could be used for RCS frames in low-to-moderate seismic regions.

Although many tests on RCS frames have been conducted, most of the tests were conducted on RCS frames with columns made of normal-strength materials. In recent years, new high-strength reinforced concrete (New RC) with $f_c^{'} \geq 70$ MPa and $f_y \geq 690$ MPa have been developed in Taiwan for high-rise reinforced concrete residential buildings [18]. The high seismic demand and high axial load for columns in high-rise buildings in Taiwan typically make the size of RC columns excessively large and the reinforcement over-crowded. High-strength materials can reduce the column size and relieve reinforcement congestion. Test results have shown New RC columns have satisfactory seismic performance [19–21] for use in regions of high seismicity.

In this research, New RC columns were combined with steel beams to form New RCS frames for use in high-rise office buildings. Two-way,

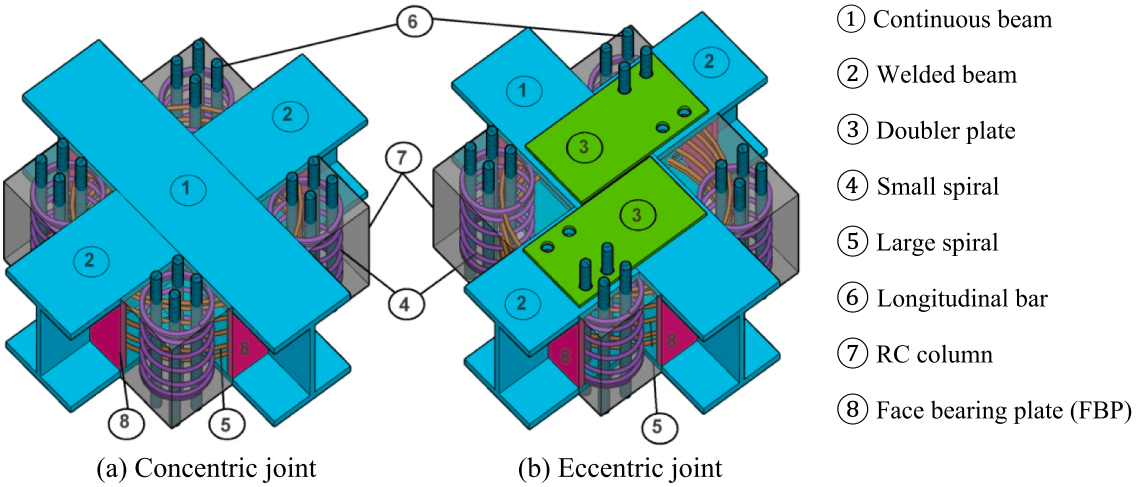

Fig. 1. Proposed joint design details: (a) concentric joint, and (b) eccentric joint.

through-beam joints were developed. Joints with beams concentrically or eccentrically connected to the joint were studied. "Two-way" means that beams frame into a column from two orthogonal sides with moment-resisting connections. Buildings in Taiwan are typically designed with two-way (space) moment-resisting frames. Most of the RCS joints studied in the literature belong to one-way (planar) frames with beams concentrically framed to the joint. In one-way frames, beams framing in from the out-of-plane direction do not transfer significant moments into the joint. In regions such as the United States, RCS joints are primarily used in one-way frames [11]. The objective of this research was to investigate the joint shear behavior of the proposed New RCS joints. Large-scale specimens were designed and tested. Test results were used to observe the joint shear behavior and examine joint shear strength models.

2. Specimen design and test setup

2.1. Proposed joint details

A two-way, through-beam joint was developed in this research, as shown in Fig. 1. "Through-beam" means that beams run through a column. In the proposed joint, the beam in one direction runs continuously through the joint. The beam in this direction is referred to as "continuous beam." The beam in the other direction is divided into two parts with the flanges and webs welded to the flanges and web of the continuous beam, respectively. The beam in this direction is referred to as "welded beam." Face bearing plates (FBPs) covering the column faces bounded by the beam flanges are used to increase the joint shear strength contributed by joint concrete, increase the joint stiffness, and provide additional concrete confinement. FBPs are the minimum attachment required by the 1994 ASCE guidelines [1] and 2015 ASCE draft Pre-Standard [11].

For transverse reinforcement in the joint region with beams framing into the joint from two orthogonal directions, previous researchers have proposed using four overlapping cross-ties [22] or four square ties [6]. The former requires predrilled holes in the webs of the beams, while the latter does not. According to the ACI 318-19 code [23], when rectilinear ties are used and when $f_c' \geq 70$ MPa or $P_u \geq 0.3A_g f_c'$, every longitudinal bar around the perimeter of the joint core needs lateral support provided by the corner of a hoop or by a seismic hook. Moreover, the amount of transverse reinforcement needs to be increased. Since $f_c' \geq 70$ MPa and $P_u \geq 0.3A_g f_c'$ are the target application range of New RCS columns, it is difficult for the joint transverse reinforcement to meet the requirement of ACI 318-19 if rectilinear ties are to be used. Therefore, five-spiral reinforcement [24–26] is proposed for the transverse reinforcement of New RCS joints. The five-spiral reinforcement consists of a large central spiral and four small corner spirals, as shown in Fig. 1. The spirals themselves can provide lateral support to every longitudinal bar around

Table 1
Specimen design parameters.

Specimen			IHS	IDEHS	ISEHS
Steel beam	Beam section (mm)		H468 × 308 × 10 × 36		
	Face bearing plate (FBP) (mm)		149 × 396 × 32		
	Thickness of flange doubler plate t_r (mm)		–	16	
	Hole diameter on beam flanges d_h (mm)		–	39	
	Length of test beam (mm) (welded beam)		2300		
RC column	f_c' (MPa)		70		
	f_{ca}' (MPa)		91.7	76.9	84.1
	Column section (mm)		800 × 800		
	Column length (mm)		3700		
	Longitudinal reinforcement		16 D32 (No. 10) SD 550 W		
	Large spiral	Column	D16 @45 mm SD 420 W, $D_L' = 720$ mm		
		Joint	D13 @85 mm SD 490 W, $D_L' = 720$ mm		
	Small spiral	Column	D10 @45 mm SD 500, $D_S' = 230$ mm		
		Joint	D12 @85 mm SD 500		
			$D_S' = 230$ mm	$D_S' = 190$ mm	
	Volumetric ratio of confinement reinforcement ρ_s (%)	Column	2.52		
		Joint	1.09	1.08	1.08

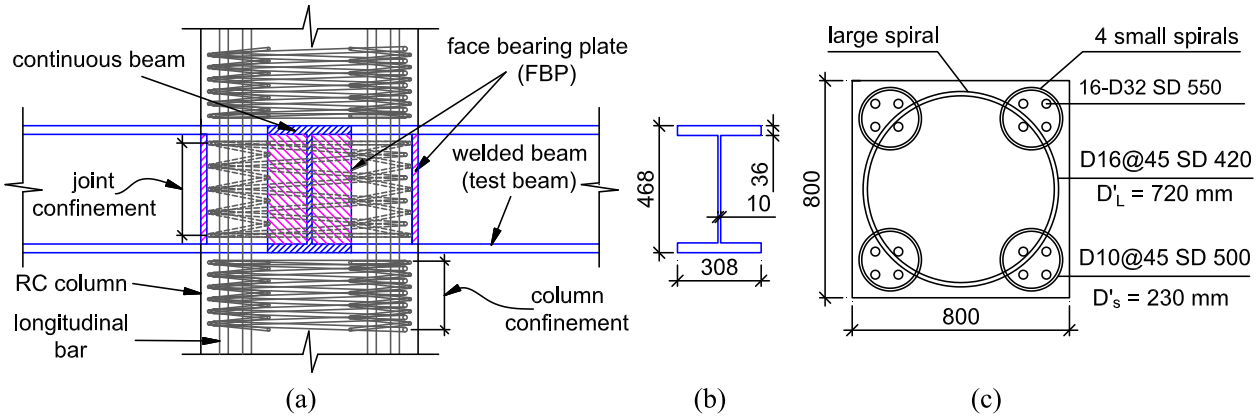

Fig. 2. Design details of column and beam of specimens: (a) elevation view of beam and column, (b) beam section, and (c) column section (Unit: mm).

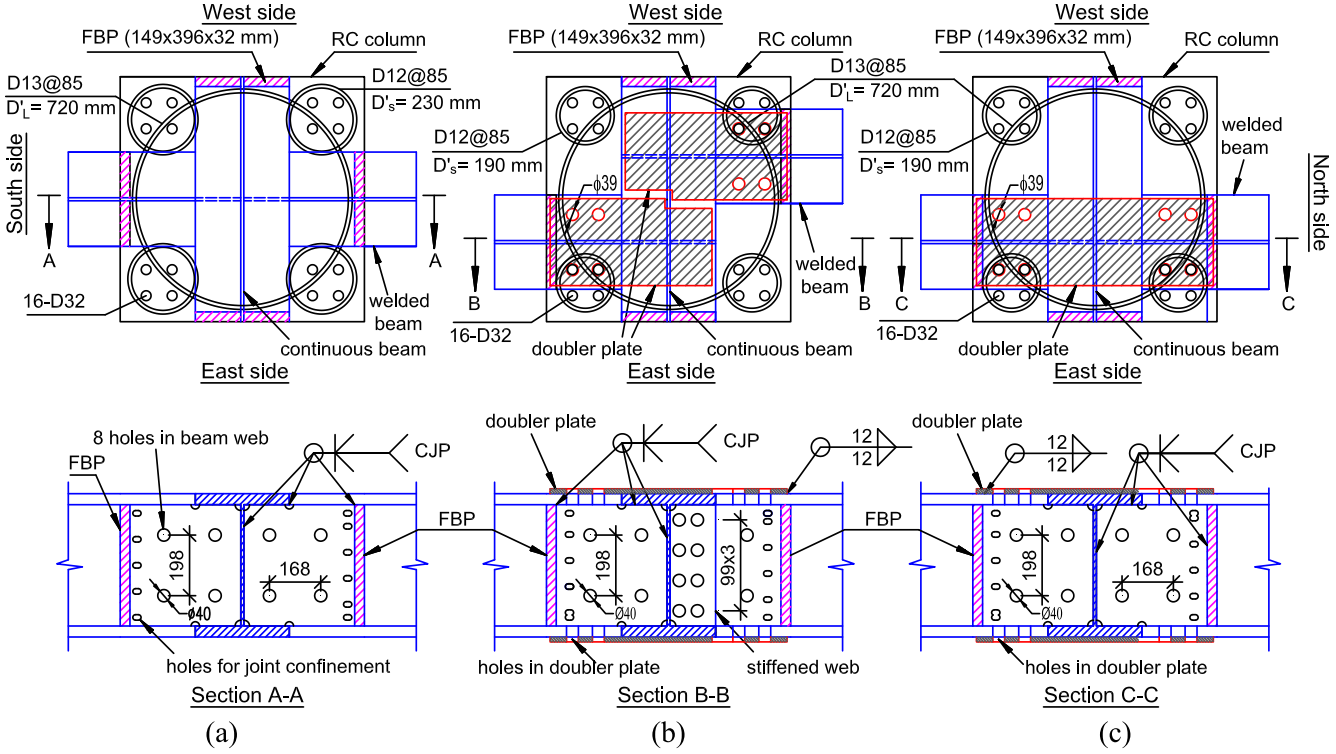

Fig. 3. Design details of joint: (a) IHS, (b) IDEHS, and (c) ISEHS.

the perimeter of the joint core. Moreover, a lower amount of reinforcement is required by ACI 318-19 for spiral reinforcement than for rectilinear tie reinforcement for the confinement design of the joint region.

In architectural design, beams may be designed to frame concentrically into the joint, as shown in Fig. 1(a). However, the beams are often required to frame eccentrically into the joint, as shown in Fig. 1(b). Eccentric RCS joints have never been studied in the literature. When beams frame eccentrically into the joint, the beams interfere with the longitudinal bars of the column. In this research, holes are predrilled in the eccentric beam flanges to allow passage of the longitudinal bars. To prevent damage to the flanges, the flanges within the joint are strengthened with doubler plates welded to the flanges. This is shown in Fig. 1(b).

2.2. Specimen design

Three large-scale specimens were designed and tested to observe the seismic shear behavior of the proposed New RCS joint. Specimen design parameters, including concrete strengths, are listed in Table 1. Design

Table 2
Specified and actual strengths of steel materials.

	SD 420 W	SD 490 W	SD 500 (D10)	SD 500 (D12)	SD 550 W	SN490B (steel flange)	SN490B (steel web)
f_y (MPa)	420	490	490	490	550	350	350
f_{ya} (MPa)	412	504	698	581	556	462	379
f_{ua} (MPa)	670	684	734	628	741	588	510

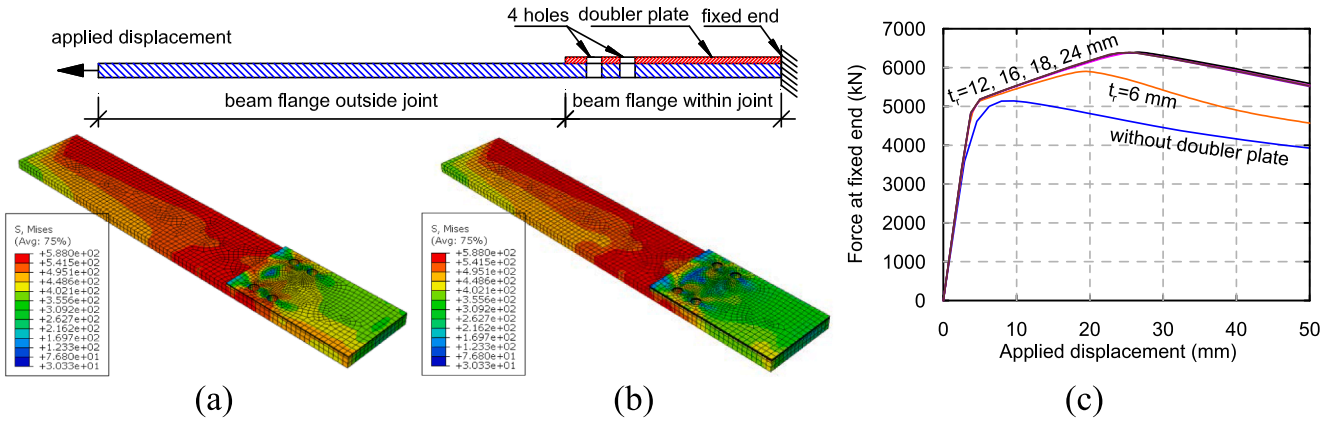

Fig. 4. (a) Finite element model with $t_r = 12$ mm, (b) finite element model with $t_r = 16$ mm, and (c) force vs. displacement relationships with various thicknesses of the doubler plate.

details of beams and columns are illustrated in Fig. 2, and those of joints are shown in Fig. 3. The yield and ultimate strengths of steel materials are listed in Table 2.

The specimens were designed so that joint shear failure would occur rather than beam hinging or joint bearing failure. Steel beams of H468 × 308 × 10 × 36 with a strength grade of SN490B were used for all three specimens. The continuous beam of each specimen was designed in the same location within the joint, from the West to East face of the column (Fig. 3). The welded beams were welded with complete joint penetration (CJP) groove welds to the continuous beam at different locations for different specimens. In specimen IHS (Interior joint, High strength, and Shear failure), the welded beams were welded concentrically to the continuous beam (Fig. 3(a)). In specimen IDEHS (Interior joint, Different sides of Eccentricity, High strength, and Shear failure), one of the welded beams was welded eccentrically to the continuous beam near the column's East face while the other near the West face of the column (Fig. 3(b)). In specimen IESHS (Interior joint, Same side of Eccentricity, High strength, and Shear failure), two welded beams were welded eccentrically to the continuous beam at the same location near the East face of the column (Fig. 3(c)). In this research, the load was applied to the welded beams because they are more critical than the continuous beam due to the presence of the welds. Hence, the continuous beam was terminated on the faces of the column. The FBPs were designed for each welded beam and for the two ends of the continuous beam. In other words, FBPs existed on the four faces of the column. The FBPs were made of SN490B steel and had a thickness of 32 mm. The thickness satisfied the 2015 ASCE draft Pre-Standard [11]. Moreover, the thickness of the beam flange within the joint also met the Pre-Standard [11].

For the eccentric joints (IDEHS and ISEHS), holes were pre-drilled to the flanges of the welded beams (Fig. 3(b) and (c)). For each flange, two holes were drilled for two longitudinal bars to pass through. Two more holes were made to prevent the flanges from being under torsion. Steel doubler plates were fillet welded to the flanges within the joint region to strengthen the flanges. The doubler plates had the same steel material as the beam flange. The thickness of each doubler plate (t_r) was selected to compensate for the maximum cross-sectional loss of the flange due to the drilled holes (A_h). Eq. (1) was proposed to determine the t_r.

$$t_r = C\frac{A_h}{b_f - \sum d_h} \tag{1}$$

The t_r depends on the number and diameter of the holes ($\sum d_h$) and a coefficient (C) to account for the effect of stress concentration around the holes. A hole diameter (d_h) of 39 mm was selected for D32 longitudinal bars (32 mm in diameter). To determine C, a three-dimensional finite element model of the beam flange was constructed by ABAQUS [27], as shown in Fig. 4(a) and (b). A portion of the model simulated the flange within the joint (with a doubler plate), and the other portion simulated the flange outside the joint. The flange and doubler plate were modeled using the 3D deformable solid. The bottom surface of the doubler plate was tied to the top surface of the flange. The steel material was modeled using the Von Mises yield criterion with an isotropic hardening property. The end of the model within the joint was fixed. The other end was subjected to a monotonically increasing displacement introducing an increasing tensile force to the flange. The value of t_r was gradually increased from 0 (without a doubler plate) to 24 mm to observe the flange's force–displacement behavior and stress distribution. Note that for $C = 1$, the t_r was determined to be 12 mm by Eq. (1). Fig. 4(c) shows the relationship between the tensile force and applied displacement of the flange. When $t_r \geq 12$ mm, the force–displacement was no longer dependent on t_r. As t_r reached 16 mm, high stresses causing yielding in the regions around the holes were significantly reduced and spread to the region outside the joint (Fig. 4(b)). Hence, C in Eq. (1) was set to 1.33, and the t_r for the doubler plate used was selected to be 16 mm.

To enable concrete vibrators to compact concrete and to allow entrapped air to leave concrete, circular holes with a diameter of 40 mm were drilled on the webs of the continuous beam and welded beams (Fig. 3). Finite element analysis was conducted to ensure the holes would not significantly affect the shear resistance of the web. Also shown in Fig. 3(b), for specimen IDEHS, the webs of the welded beams were extended to the other side of the web of the continuous beam to enhance the bearing resistance of the flanges and to increase the stiffness of the connection between the welded beam and continuous beam.

The high-strength concrete columns were designed following the ACI 318-19 code [23]. The columns had a square cross-section of 800 × 800 mm and a height of 3700 mm for all three specimens. The specified compressive strength of concrete (f_c') was 70 MPa. The actual compressive strength (f_{ca}') for each specimen on the test day is listed in Table 1. As shown in Fig. 2, sixteen D32 SD 550W deformed bars were used as longitudinal reinforcement, resulting in a longitudinal reinforcement ratio of 2.04%.

Five-spiral reinforcement was used as transverse reinforcement. For the column portions outside the joint region, D16 SD 420W and D10 SD 500 deformed bars were used for the large and small spirals, respectively, of the five-spiral reinforcement. The outer diameters of the large and small spirals were 720 mm and 230 mm, respectively. According to the ACI 318-19 code [23], for columns of special moment frames, the minimum amount of confinement reinforcement ($\rho_{s,ACI}$) for the potential plastic hinge region should be the greatest of values given by Eqs. (2), (3), and (4) when $f_c' \geq 70$ MPa.

$$\rho_{s,ACI} = 0.45\left(\frac{A_g}{A_{ch}} - 1\right)\frac{f_c'}{f_{yt}} \tag{2}$$

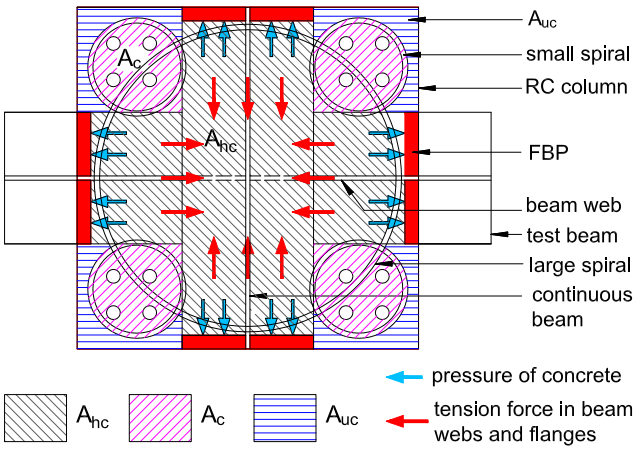

Fig. 5. Confined and unconfined regions of joint.

$$\rho_{s,ACI} = 0.12\frac{f_c'}{f_{yt}} \tag{3}$$

$$\rho_{s,ACI} = 0.35k_f\frac{P_u}{f_{yt}A_{ch}}$$

$$k_f = \frac{f_c'}{175} + 0.6 \geq 1.0 \tag{4}$$

Note that A_{ch} is the area enclosed by the outside edges of the five spirals. $\rho_{s,ACI}$ needs to be satisfied for each spiral. Based on Eqs. (2), (3), and (4), the vertical spacing of the spirals outside the joint was selected to be 45 mm (ρ_s = 2.52%). The shear strength of the five-spiral reinforcement was calculated based on the discrete computational shear strength model [26]. The design shear strength of the column was sufficient to ensure no shear failure of the column would occur. The amount of confinement above and below the beam flanges satisfied the 2015 ASCE draft Pre-Standard [11].

According to the ACI 318-19 code [23], transverse reinforcement in the joint must satisfy Eqs. (2), (3), and (4). Moreover, according to the 1994 ASCE Guidelines [1]. The ratio of the net area to the gross area of the web should be greater than 0.7. For the proposed two-way New RCS joint to satisfy the amount of transverse reinforcement required by ACI 318-19, very dense holes would be needed on the webs for the passage of transverse reinforcement, which would violate the 1994 ASCE guidelines on the net web area. In this research, a reduction in the amount of transverse reinforcement was proposed for the large spiral considering the confinement effect from the FBPs. The proposed reduced amount of transverse reinforcement ($\rho_{s,prop}$) is defined by Eqs. (5) and (6). Note that only the amount of the large spiral was reduced by Eq. (5), while the amount of the small spirals was not reduced. This is because most of the area confined by FBPs is within the confined area of the large spiral.

$$\rho_{s,prop} = \gamma \times \rho_{s,ACI} \tag{5}$$

$$\gamma = \frac{A_c + A_{uc}}{A_{hc} + A_c + A_{uc}} \tag{6}$$

The concrete in the joint region is divided into three distinct areas, the one confined by the FBPs and beam webs and flanges (A_{hc}), the one confined only by five-spiral reinforcement (A_c), and the remaining unconfined concrete area (A_{uc}), as demonstrated in Fig. 5. It is proposed that the minimum amount of transverse reinforcement required by ACI 318-19 ($\rho_{s,ACI}$) can be reduced by a coefficient γ, which is defined by Eq. (6). In Eq. (6), it is assumed that the FBPs interconnected by webs and flanges of the beams can provide sufficient confinement to the area A_{hc} so that this area can be removed from the confinement calculation. As shown in Fig. 5, confining pressures from concrete are resisted by tension forces developed in the beam webs and top and bottom flanges. FBPs act as "slabs" to take and transfer the confining pressures from the concrete to the steel webs and flanges. Based on the proposed equation (Eq. (5)), D13 SD 490W and D12 SD 500 deformed bars were used for large and small spirals, respectively, for the joint region. The spacing of the spirals was selected to be 85 mm, which resulted in a volumetric ratio ρ_s = 1.1%. The amount of transverse reinforcement in the joint region was 52% of that in the column. Note that for the eccentric joints (IDEHS and ISEHS), the outer diameter of the small spirals in the joint region was reduced from 230 mm to 190 mm to fit into the reduced corner space due to the eccentricity of the welded beams.

2.3. Construction of specimens

Fig. 6 depicts the construction of the specimens. The steel components, including the continuous steel beam, welded beams, face bearing plates, and doubler plates (used only for eccentric joints) were first welded. Then, the large spiral was inserted through the predrilled holes in the beam webs within the joint. And, the small spirals were placed within the joint, interlocking with the large spiral. Finally, the steel reinforcement of the column outside the joint was fabricated before the steel formwork was built for concrete casting.

2.4. Test setup

The specimens were tested at National Center for Research on Earthquake Engineering (NCREE), Taiwan (Fig. 7). The upper end of the column was pin connected to two horizontal actuators, which were used to fix the horizontal movement of the upper end of the column during testing. The lower end of the column was tied in a way to simulate a pin connection to a steel frame fixed to the strong floor. The length of the column from the center of the upper pin to the lower pin was 3200 mm, representing the distance between the inflection points of the column under seismic loading. Axial compression of 5 %$A_g f_{ca}'$ was applied to the top end of the column and maintained constant throughout testing. This low level of axial compression was not intended to simulate the axial

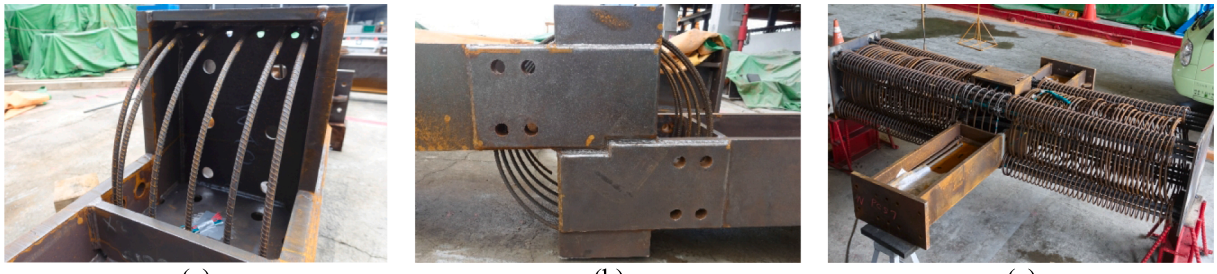

Fig. 6. Construction of specimens: (a) large spirals within the joint, (b) the doubler plates (eccentric joints), and (c) steel beams and reinforcement cage of the column.

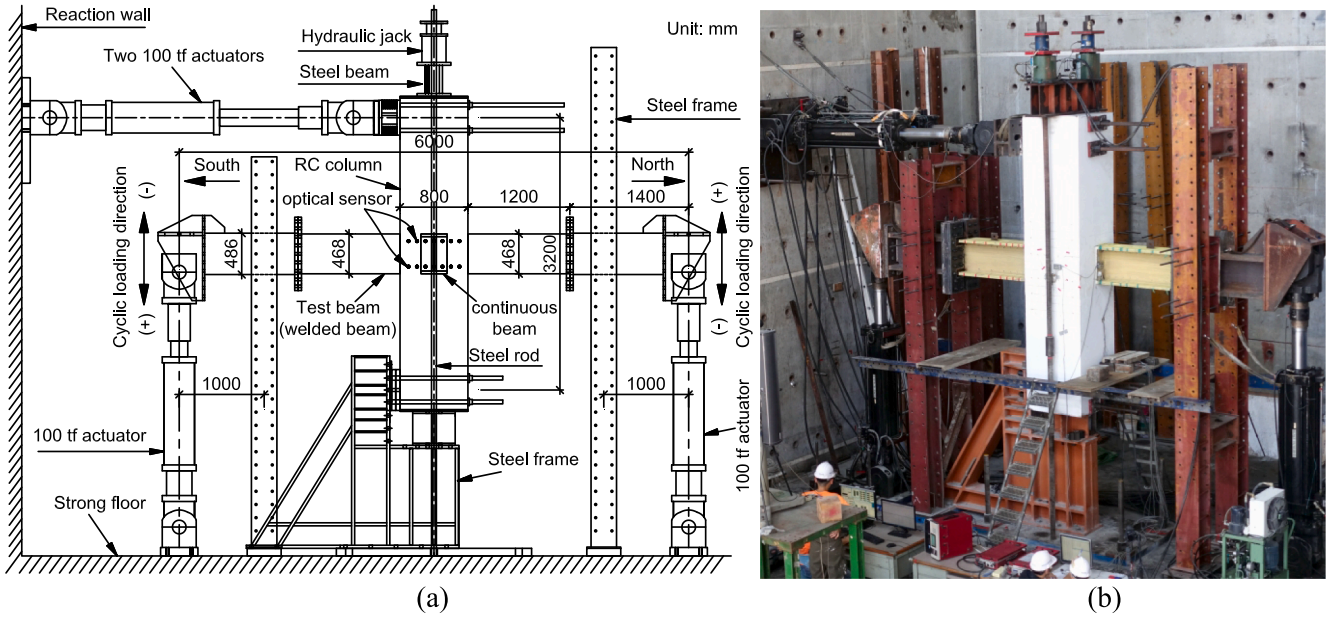

Fig. 7. (a) Test setup, and (b) photo of test setup (north-east side view).

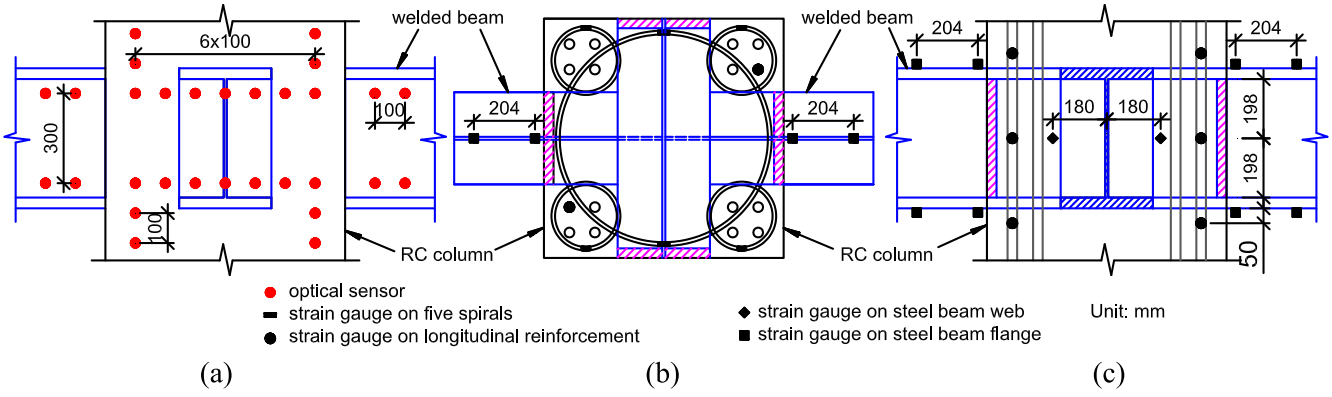

Fig. 8. (a) Location of optical sensors (east side), (b) location of strain gauge (plan view), and (c) location of strain gauge (elevation view).

load of the column but to stabilize the test setup and to provide a conservative test value of joint shear strength.

Two test beams (welded beams), referred to as north and south beams, framed into the joint. Each test beam was divided into two parts. The first part was connected to the joint. The second part was connected to the first part with bolts and was reused for every specimen. Cyclic loading was applied to the free ends of the test beams using vertical actuators to drift levels of 0.25%, 0.375%, 0.5%, 0.75%, 1%, 1.5%, 2%, 3%, 4%, 5%, 6%, 7%, 8%, 9%, and 10%. The two vertical actuators moved in opposite directions to simulate beam movement during an earthquake. The drift level was determined by dividing the relative vertical displacement of the two vertical actuators by the distance between the loading points of the two actuators (6000 mm). Note that loading was applied at the beam ends, so the drift level represents the beam drift level rather than the column drift level [28,29]. The effect of loading at beam ends or column ends on the behavior of beam-column joints can be found in Yang et al. [30]. Each drift level has positive and negative drift ratios. A positive drift ratio means the actuator at the north beam end moving up and that at the south beam end moving down. Each drift level was repeated three times to observe the degradation of stiffness and strength of the joint. Two additional steel frames were attached to the strong floor and positioned at 1000 mm from each vertical actuator to provide lateral support to the test beams.

The applied forces and displacements of the actuators were recorded. An optical motion tracking system was used to measure the deformation of the joint and test beams. Sensors were attached to the east face of the joint and the test beams for the optical system to monitor the displacements of the sensor locations (Fig. 8(a)). Strain gauges were installed on the test beams and the longitudinal and transverse reinforcement of the column. Locations of the strain gauges are illustrated in Fig. 8(b) and (c).

3. Test results and discussion

3.1. Crack patterns and damages condition

For all three specimens, at early drift levels (0.5–0.75%), horizontal cracks occurred in the column near the flanges of the test beams. These cracks were due to the flexural tensile stresses induced by the column moment above and below the joint and soon stabilized. Cracks also occurred on the east and west faces of the column radiating from the corners of the continuous beam. These cracks were due to the rotation of the continuous beam mobilized by the movement of the test beams. As the drift levels increased to 0.75–1.0%, diagonal cracks appeared on the east and west faces of the column on the two sides of the continuous beam. As the drift level increased, the number of cracks increased. Moreover, the cracks gradually propagated into the column regions

Table 3
Peak applied load and joint shear.

Specimen	Peak total applied load				Peak joint shear (kN)			Joint shear at 0.5% shear deformation (kN)			$\frac{V_{test\_0.5}}{V_{test}}$
	+		−		+	−	Average (V_{test})	+	−	Average ($V_{test\_0.5}$)	
	Drift (%)	Force (kN)	Drift (%)	Force (kN)							
IHS	5.01	1673	−5.00	1655	8509	8436	8472	7681	7818	7749	0.91
IDEHS	6.00	1803	−5.98	1813	9319	9373	9346	8490	7862	8176	0.87
ISEHS	6.00	1696	−4.99	1699	8671	8852	8761	7171	6419	6795	0.78

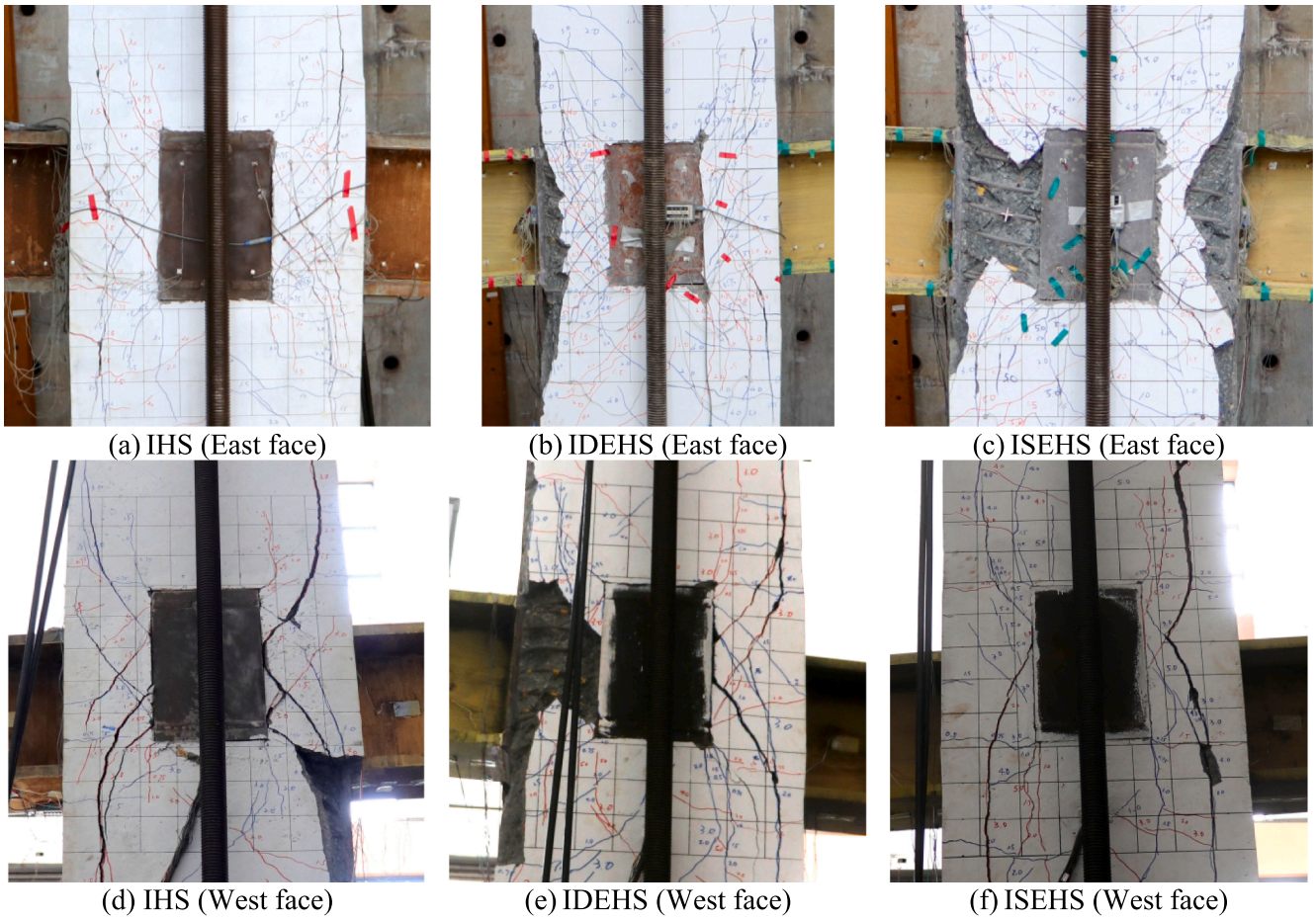

Fig. 9. Damage of joint at the peak load: (a) IHS (East face), (b) IDEHS (East face), (c) ISEHS (East face), (d) IHS (West face), (e) IDEHS (West face), and (f) ISEHS (West face).

approximately 300–400 mm above and below the steel beam flanges. These diagonal cracks showed that the outer concrete panel was mobilized to resist the joint shear. The outer concrete panel was likely mobilized by the combined effect of the continuous beam (transverse beam) and the friction between the beam flange and concrete in the vertical bearing region. At 3–5%, spalling of concrete occurred starting from the corners of the column, followed by spalling on the east and west faces of the column around the continuous beam. Spalling was first seen in ISEHS at 3%, earlier than in IHS and IDEHS, for which spalling started at 4%. The eccentricity of both welded beams to the same side (east face) of ISEHS created higher shear demand to that side of concrete and hence induced earlier spalling.

For specimen IHS, the total applied load (summation of the applied load of the north beam actuator (positive for "push") and that of the south beam actuator (positive for "pull")) reached the peak at a drift level of 5% (Table 3). The damage condition is shown in Fig. 9(a) (east face) and (d) (west face). Significant diagonal cracks and some spalling of concrete can be seen. For specimen IDEHS, the total applied load reached the peak load at a drift level of 6%. The damage condition is shown in Fig. 9(b) (east face) and (e) (west face). Both the photos show more damage on the left side because the test beam framed into the joint eccentrically closer to that side. For specimen ISEHS, the total applied load reached the peak at a drift of 6% for positive drift ratios and 5% for negative drift ratios. The damage condition at a drift level of 5% is shown in Fig. 9(c) (east face) and (f) (west face). The east face of the column suffered more damage than the west face because the test beams framed to the joint eccentrically closer to the east face than the west face.

At a drift level of 7%, gaps were visible between beam flanges and column concrete for specimen IHS. The gaps were caused by the vertical movement of the steel beam flanges relative to the column concrete. However, the core concrete of the column did not crush under the push of the beam flange until the end of the test at a drift level of 10%. The peak total applied load at a drift level of 10% had dropped to 62% of all

Fig. 10. Damage of joint at test end: (a) IHS, (b) IDEHS, and (c) ISEHS.

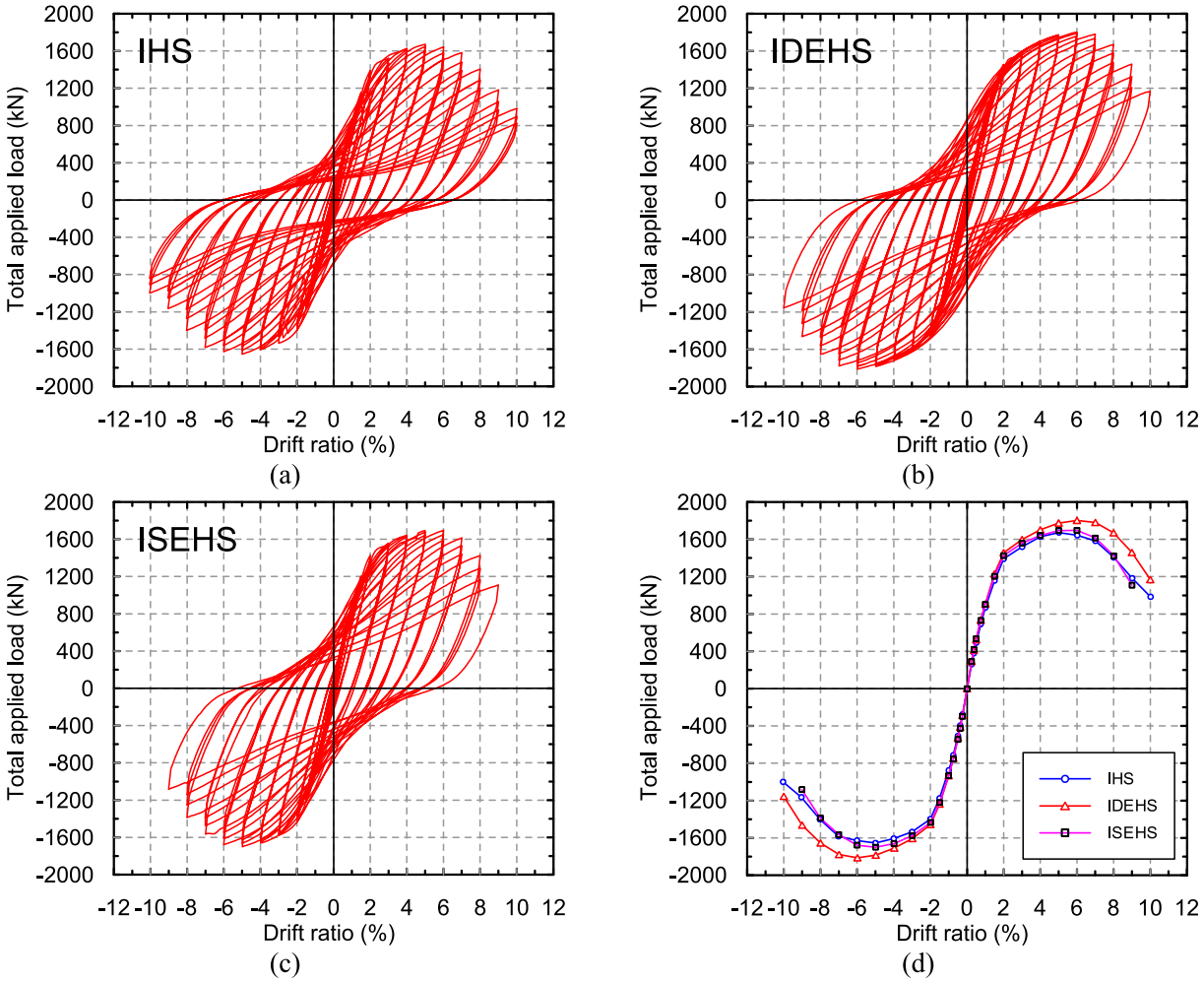

Fig. 11. Hysteresis response: (a) IHS, (b) IDEHS, (c) ISEHS, and (d) envelope response.

drift levels' peak total applied load. The gaps were also seen for specimens IDEHS and ISEHS but were less pronounced. This was likely due to the strengthening effect of the column longitudinal bars that passed through the flanges on the vertical bearing capacity between the beam flanges and concrete. Specimen IDEHS was terminated at a drift level of 10%. The total peak applied load at that drift level had dropped to 66% of all drift levels' peak total applied load. The strength degradation of specimen ISEHS was faster than the other two specimens. Hence, the test was terminated earlier at a drift level of 9% when the peak total applied load had dropped to 65% of all drift levels' peak total applied load. For this specimen, both the test beams were eccentric to the same side of the joint, causing more severe damage to one side than the other two

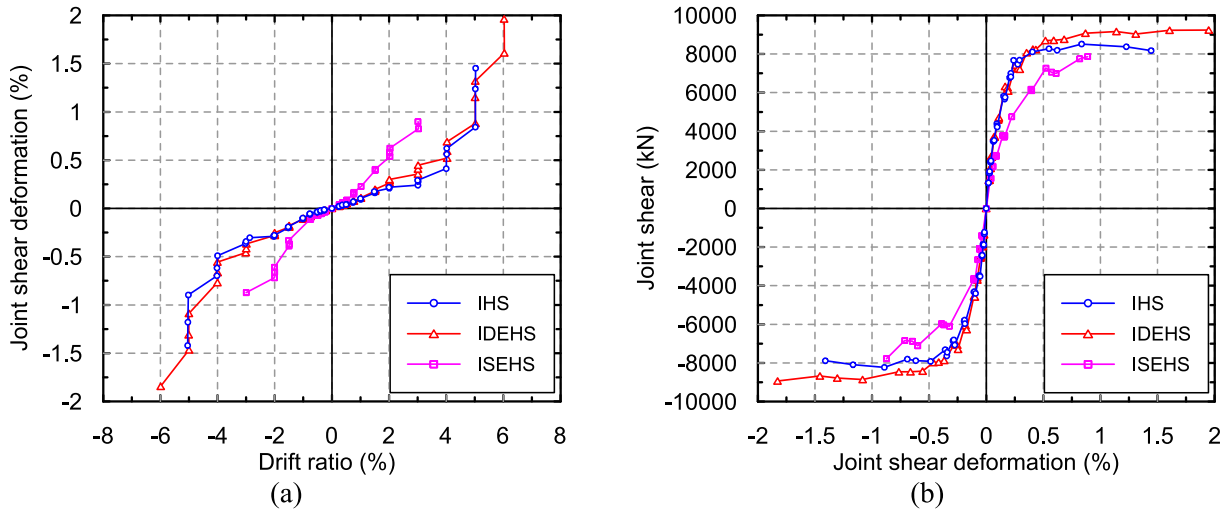

Fig. 12. Envelope responses for (a) joint shear deformation and drift ratio; and (b) joint shear and joint shear deformation.

specimens, thus resulting in a faster strength degradation.

Fig. 10 shows the damage conditions of all three specimens at the test end. All the specimens failed due to joint shear. Spalling of cover concrete and crushing of core concrete in the joint's outer and inner concrete panels were seen. Spirals and longitudinal bars within the joint were exposed. No fracture of transverse reinforcement within the joint was found except that one fracture was found for one small spiral of IDEHS. After removing the joint concrete, the webs of the test beams were found to fracture. No visible damage was found to the CJP welds connecting the test beams to the continuous beam. The flanges of the eccentric test beams did not show any fracture around the holes. The doubler plates were effective in protecting the flanges with holes. The FBPs and the surrounding welds were all not damaged.

No obvious sign of bearing failure was observed. Spalling of concrete was found above and below the joint. However, the spalling was primarily limited to the cover concrete. Note that the damage condition presented in Fig. 10 was at the end of the test (drift levels of 9–10%). When the specimens reached the joint shear strength (peak load) at drift levels of 5–6%, as shown in Fig. 9, the damage to cover concrete right above and below the joint was much less. These findings confirmed that the specimen failed due to joint shear rather than bearing.

3.2. Hysteresis responses and force-drift envelope

The hysteretic and envelope responses between the total applied load and drift ratio of all three specimens are shown in Fig. 11. The values of the peak total applied loads are listed in Table 3. Interestingly, the eccentric specimens (IDEHS and ISEHS) showed 10.3% and 3.4% higher average joint shear strength than the concentric specimen (IHS). This was likely due to the strengthening effect of column longitudinal bars that passed through the beam flanges of the eccentric specimens. Those bars increased the joint shear strength by providing dowel actions to resist the shearing movement of beam flanges. Moreover, the doubler plates increased the stiffness against bending of the beam within the joint and could better maintain the concrete strut of the inner panel to resist joint shear. The average joint shear strength of IDEHS was higher than that of ISEHS by 6.7%. This was likely because the test beams of IDEHS were eccentric to different sides within the joint, which spread the damage to different sides of the joint. In contrast, the test beams of ISEHS were eccentric to the same side within the joint, which made the damage concentrated to one side (Fig. 9). This reduced the joint shear strength compared with IDEHS. Moreover, the concentration of damage to one side degraded the joint shear strength faster than in the other two specimens. This can be seen in Fig. 11(d). As a result, testing of ISEHS was terminated 1% drift level earlier than the other two specimens, as stated previously. One more possible reason for IDEHS to show the highest joint shear strength was that the total length of steel webs of the test beams within the joint was the largest, as shown in Fig. 3.

The peak values of joint shear forces are listed in Table 3. Joint shear deformation was calculated using the recorded data from the optical motion tracking system stated previously. The envelope responses between the drift ratio and joint shear deformation of all three specimens are shown in Fig. 12(a). Due to the earlier damage to the east face of specimen ISEHS, the sensors measuring the deformation of the joint were removed earlier than those of the other two specimens. Thus, the curve for ISEHS in Fig. 12(a) was terminated earlier. The joint shear deformation of this specimen (ISEHS) increased faster than the other two specimens. The envelope responses between the joint shear and joint shear deformation of all three specimens are shown in Fig. 12(b). The joint shear corresponding to 0.5% joint shear deformation for each specimen was identified in Fig. 12(b) and listed in Table 3 ($V_{test\_0.5}$). According to Parra and Wight [12], the joint shear deformation can be limited to 0.5% to limit the joint damage. Fig. 12(b) shows that significant softening in responses occurred after 0.5% joint shear deformation.

3.3. Strain responses

The strain responses from various locations are presented in Fig. 13. Also indicated in the figure are the drift corresponding to 0.5% joint shear deformation and peak joint shear. In some plots, responses were not shown for all the specimens because of the malfunction of the strain gauges. The steel web within the joint reached shear yielding before peak joint shear (Fig. 13(a)). This means the full yield strength of the web can be used for joint shear strength calculation. The shear strain of IDEHS was smaller than IHS for the same drift ratio. This was due to the increased joint shear resistance due to column longitudinal bars that passed through the flanges of the test beams and a longer total length of steel webs within the joint.

The large spiral within the joint showed yielding before the peak joint shear was reached (Fig. 13(b)). The strain increased rapidly after yielding. The large spiral appeared to be fully mobilized to provide confinement and resist joint shear. Note that no fracture of large spirals was found at the end of the test, as stated previously. The small spiral within the joint was less mobilized but still showed strain responses exceeding or close to yielding at the peak joint shear (Fig. 13(c)). The column longitudinal reinforcement outside but close to the joint slightly exceeded yielding (IHS and ISEHS) or close to yielding (IDEHS) (Fig. 13(d)). Significant flexural yielding did not occur in the column as intended in the design. The beam flanges outside but close to the joint exceeded yielding before the peak joint shear for all specimens (Fig. 13

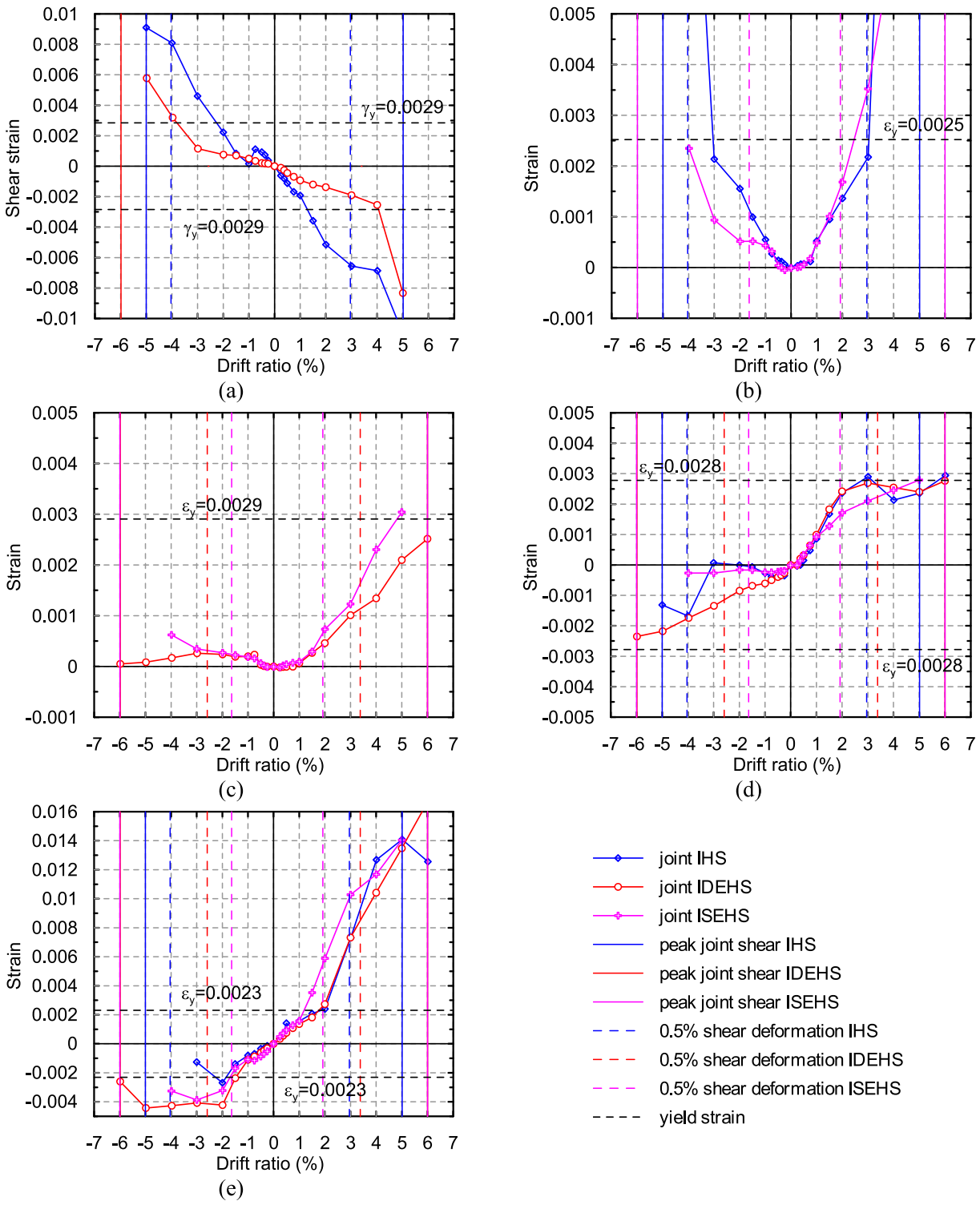

Fig. 13. Envelope of strain responses: (a) steel web in the joint, (b) large spiral in the joint, (c) small spiral in the joint, (d) longitudinal reinforcement of the column close to the joint, and (e) steel beam flange close to the column.

(e)). However, the yielding was not significant enough to cause any distortion or buckling of the flanges until the end of the test, as shown in Fig. 10.

4. Shear strength models for joints

The measured beam peak moment, peak joint shear, and joint shear at 0.5% joint deformation were compared to the analytical flexural strength of the beam, and the analytical bearing strength and shear strength of the joint. The joint shear strength and bearing strength models from the 1994 ASCE guidelines (V_{n1} and V_{b1}, respectively) [1] and those from the 2015 ASCE draft Pre-Standard (V_{n2} and V_{b2}, respectively) [11] were examined. The equations of the models are listed in Table 4. The results of the comparison are listed in Table 5. The measured average peak moment (M_{test}) was close to or slightly exceeding the nominal moment strength of the beam based on actual material

Table 4
Joint shear and bearing strength equations (stress in MPa).

	1994 ASCE guidelines [1]	2015 ASCE draft Pre-Standard [11]
V_n	$V_{n1} = V_{spn1} + V_{icn1} + V_{on1}$	$V_{n2} = V_{spn2} + V_{icn2} + V_{on2}$
V_{spn}	$V_{spn1} = 0.6F_{ysp}t_{sp}jh$	$V_{spn2} = 0.6\alpha_{sp}F_{ysp}t_{sp}h$ $\alpha_{sp} = 0.9$: interior joints $\alpha_{sp} = 0.8$: exterior joints
V_{icn}	$V_{icn1} = 1.7\sqrt{f_c'}b_p h \le 0.5f_c' b_p d_w$	$V_{icn2} = 1.7\alpha_c\sqrt{f_c'}b_i h \le 0.5f_c' b_f d_j$ $\alpha_c = 1$: interior joints $\alpha_c = 0.6$: exterior joints
V_{on}	$V_{on1} = 1.7\sqrt{f_c'}b_o h$	$V_{on2} = 1.25\alpha_c\sqrt{f_c'}b_o h$
V_b	$V_{b1} = \frac{M_{vb1} - V_{beam,test}h}{d_j}$ $M_{vb1} = C_{cn1}h(1-\beta_1/2)$ $C_{cn1} = 2f_c' b_j(\beta_1 h/2)$	$V_{b2} = \frac{M_{vb2} - V_{beam,test}h}{d_j}$ $M_{vb2} = C_{cn2}h(1-\beta_1^*/2)$ $C_{cn2} = 2f_c' b_f(\beta_1^* h/2)$

properties ($M_{p,actual}$). The average value of $M_{test}/M_{p,actual}$ was 0.96. The measured peak joint shear (V_{test}) was much less than the shear corresponding to the bearing capacity between the beam flange and the column (V_{b1} and V_{b2}) for all the specimens. The average values of V_{test}/V_{b1} and V_{test}/V_{b1} were 0.62 and 0.59, respectively. These comparison results are consistent with the test observations that the failure of the specimens was not governed by the flexural failure of the beam nor the bearing failure between the beam flange and the column.

The values of V_{test}/V_{n1} and V_{test}/V_{n2} were larger than 1.0 for all the specimens with an average value of 1.73 and 1.46, respectively. The joint shear strength models from the 1994 ASCE guidelines and 2015 ASCE draft Pre-Standard provided conservative predictions of peak joint shear for all the specimens, including the eccentric specimens. However, predictions by the 1994 ASCE method were too conservative. This is mainly due to two reasons. One is that in V_{n1}, the shear strength contribution of the outer joint panel can only be mobilized by shear keys (steel columns or extended FBPs), which were not used in the specimens tested. In contrast, in V_{n2}, the shear strength contribution of the outer joint panel can also be mobilized by the friction between the beam flange and concrete in the vertical bearing region. The second reason is the V_{n2} allows a longer steel web within the joint to be used in shear strength calculation. The 2015 ASCE method produced predictions that were reasonably conservative and with less scatter (a smaller COV) than the 1994 ASCE method.

The average values of $V_{test\_0.5}/V_{n1}$ and $V_{test\_0.5}/V_{n2}$ were 1.47 and 1.25, respectively. Both joint shear strength models can provide conservative predictions even for joint shear corresponding to 0.5% joint shear deformation. In other words, the damage of joints with the proposed design details is expected to be limited if designed with any of the two models. As stated in the 2015 ASCE draft Pre-Standard [11], a coefficient k of 0.85 can be used to reduce the joint shear strength to limit the joint deformation. Therefore, $V_{test\_0.5}$ was further compared with $0.85V_{n2}$. The average value of $V_{test\_0.5}/0.85V_{n2}$ was 1.47 (Table 5), similar to the average value of V_{test}/V_{n2} (1.46). This is because the average value of $V_{test\_0.5}/V_{test}$ was 0.853 (Table 5), close to k (0.85). This means the value of k may be appropriate for the proposed joint details to further control the joint deformation. However, note that the value of $V_{test\_0.5}/V_{test}$ for ISEHS was 0.78, lower than the value of k.

5. Conclusion

New high-strength reinforced concrete column and steel beam (New RCS) joints were proposed. The proposed joints used high-strength concrete and reinforcement for columns. New through-beam joint details were developed, including two-way joint connection, five-spiral reinforcement for joint confinement, and eccentric joint details. Large-scale New RCS specimens were designed to fail in joint shear and tested. Important conclusions are summarized as follows.

(1) All the specimens showed joint shear failure characterized by crushing of joint concrete, yielding of joint transverse reinforcement, and fracture of steel webs within the joint. With the proposed joint details, all specimens reached high drift ratios (10% for IHS and IDEHS and 9% for ISEHS) before the test was terminated. The five-spiral reinforcement with the proposed amount provided sufficient confinement and shear resistance to the joint. The welded connection joining the welded beams (test beams) to the continuous beam did not show any fracture for all the specimens. For the eccentric specimens (IDEHS and ISEHS), the beam flanges with predrilled holes strengthened by doubler plates did not show any fracture around the holes. The proposed design method for the doubler plate was effective.
(2) The eccentric joint specimens (IDEHS and ISEHS) exhibited 10.3% and 3.4% higher peak joint shear than the concentric joint specimen (IHS). This was likely due to the strengthening effect of column longitudinal reinforcement that passed through the beam flanges and the doubler plates used to strengthen the beam flanges within the joint. The specimen with the test beams eccentric to the same side of the joint (ISEHS) showed a faster strength degradation and faster increase of joint shear deformation because the damage was concentrated on one side of the joint. Although this specimen (ISEHS) showed a higher peak joint shear, the joint shear corresponding to 0.5% joint shear deformation was lower than the concentric specimen (IHS).
(3) Both the 1994 ASCE and 2015 ASCE models provided conservative predictions of joint shear strength to all the specimens. However, the predictions by the 1994 ASCE were too conservative. The shear strength contribution from the outer joint panel was ignored for all the specimens because no steel columns or extended FBPs were used as shear keys. The 2015 ASCE method produced more reasonable predictions with less scatter by considering the shear strength contribution from the outer joint panel and allows a longer steel web in shear strength calculation. Both methods, without any reduction to limit the joint deformation, also produced conservative predictions for the joint shear strength corresponding to 0.5% joint shear deformation. The strength reduction factor of 0.85 to limit the joint deformation specified in the 2015 ASCE method may be appropriate for the proposed joint details.

Data Availability Statement

Some or all data, models, or code generated or used during the study are available from the corresponding author by request.

Table 5
Comparison of test results with analytical strengths.

	V_{n1} (kN)	V_{n2} (kN)	V_{b1} (kN)	V_{b2} (kN)	M_{test} (kN)	V_{test} (kN)	$V_{test\_0.5}$(kN)	$\frac{M_{test}}{M_{p,actual}}$	$\frac{V_{test}}{V_{b1}}$	$\frac{V_{test}}{V_{b2}}$	$\frac{V_{test}}{V_{n1}}$	$\frac{V_{test}}{V_{n2}}$	$\frac{V_{test\_0.5}}{V_{n1}}$	$\frac{V_{test\_0.5}}{V_{n2}}$	$\frac{V_{test\_0.5}}{0.85V_{n2}}$
IHS	5389	6274	16,024	16,808	2168	8472	7749	0.92	0.53	0.50	1.57	1.35	1.44	1.24	1.45
IDEHS	4903	5884	13,030	13,688	2391	9346	8176	1.01	0.72	0.68	1.91	1.59	1.67	1.39	1.63
ISEHS	5156	6078	14,504	15,224	2242	8761	6795	0.95	0.60	0.58	1.70	1.44	1.32	1.12	1.32
Average								0.96	0.62	0.59	1.73	1.46	1.47	1.25	1.47
COV								0.05	0.15	0.15	0.10	0.08	0.12	0.11	0.11

CRediT authorship contribution statement

Yu-Chen Ou: Conceptualization, Methodology, Resources, Writing – review & editing, Supervision, Project administration, Funding acquisition. **Nguyen Van Bao Nguyen:** Methodology, Software, Validation, Formal analysis, Investigation, Data curation, Writing – original draft, Visualization. **Wei-Ru Wang:** Methodology, Validation, Formal analysis, Investigation, Data curation, Visualization.

Declaration of Competing Interest

The authors declare that they have no known competing financial interests or personal relationships that could have appeared to influence the work reported in this paper.

Acknowledgements

The authors would like to thank the support from the Ministry of Science and Technology of Taiwan under Contract No. 109-2221-E-002-003-MY3, from the Ruentex Engineering & Construction Co., Ltd of Taiwan, and from National Center for Research on Earthquake Engineering (NCREE) of Taiwan.

References

[1] ASCE Task Committee on Design Criteria for Composite Structures in Steel and Concrete. Guidelines for design of joints between steel beams and reinforced concrete columns. J Struct Eng ASCE 1994; 120(8):2330-57.
[2] Sheikh TM, Deierlein GG, Yura JA, Jirsa JO. Beam-column moment connections for composite frames: Part 1. J Struct Eng ASCE 1989;115(11):2858–76.
[3] Deierlein GG, Sheikh TM, Yura JA, Jirsa JO. Beam-column moment connections for composite frames: Part 2. J Struct Eng ASCE 1989;115(11):2877–96.
[4] Kanno R, Deierlein GG. Strength, deformation, and seismic resistance of joints between steel beams and reinforced concrete columns. Structural Engrg. Report No. 93-6, Cornell University, Ithaca, N.Y; 1993.
[5] Parra-Montesinos G, Wight JK. Seismic response of exterior RC column-to-steel beam connections. J Struct Eng ASCE 2000;126(10):1113–21.
[6] Cheng CT, Chen CC. Seismic behavior of steel beam and reinforced concrete column connections. J Constr Steel Res 2005;61(5):587–606.
[7] Liang X, Parra-Montesinos GJ. Seismic behavior of reinforced concrete column-steel beam subassemblies and frame systems. J Struct Eng 2004;130(2):310–9.
[8] Deierlein GG, Noguchi H. Overview of U.S.–Japan research on the seismic design of composite reinforced concrete and steel moment frame structures. J Struct Eng ASCE 2004;130(2):361–7.
[9] Parra-Montesinos G, Wight JK. Modeling shear behavior of hybrid RCS beam-column connections. J Struct Eng ASCE 2001;127(1):3–11.
[10] Kanno R, Deierlein GG. Design model of joints for RCS frames. Composite construction in steel and concrete IV, Proceedings of the conference, Alberta, Canada 2002; 947–58.
[11] Kathuria D, Miyamoto International Inc, Yoshikawa H, Nishimoto S, Kawamoto S, Taisei Corp., Deierlein GG. Design of composite RCS special moment frames. Report No. 189, The John A. Blume Earthquake Engineering Center, Stanford University; 2015.
[12] Parra-Montesinos GJ, Liang X, Wight JK. Towards deformation-based capacity design of RCS beam–column connections. Eng Struct 2003;25(5):681–90.
[13] Alizadeh S, Attari NKA, Kazemi MT. Experimental investigation of RCS connections performance using self-consolidated concrete. J Constr Steel Res 2015;114:204–16.
[14] Mirghaderi SR, Bakhshayesh Eghbali N, Ahmadi MM. Moment-connection between continuous steel beams and reinforced concrete column under cyclic loading. J Constr Steel Res 2016;118:105–19.
[15] Bakhshayesh Eghbali N, Mirghaderi SR. Experimental investigation of steel beam to RC column connection via a through-plate. J Constr Steel Res 2017;133:125–40.
[16] Khaloo A, Bakhtiari Doost R. Seismic performance of precast RC column to steel beam connections with variable joint configurations. Eng Struct 2018;160:408–18.
[17] Lee HJ, Park HG, Hwang HJ, Kim CS. Cyclic lateral load test for RC column–steel beam joints with simplified connection details. J Struct Eng ASCE 2019;145(8): 04019075. https://doi.org/10.1061/(ASCE)ST.1943-541X.0002369.
[18] Taiwan New RC Guidelines. Design guidelines for building of high-strength reinforced concrete structures (Draft). National Center for Research on Earthquake Engineering (NCREE), Taiwan; 2019. p. 125.
[19] Ou YC, Alrasyid H, Haber ZB, Lee HJ. Cyclic behavior of precast high-strength reinforced concrete columns. ACI Struct J 2015;112(6):839–50.
[20] Ou YC, Alrasyid H, Nguyen NVB. Minimum shear reinforcement for columns with high-strength reinforcement and concrete. J Struct Eng 2021;147(2):04020313. https://doi.org/10.1061/(ASCE)ST.1943-541X.0002854.
[21] Ou YC, Nguyen NVB. Stress limit for shear reinforcement of high-strength columns. ACI Struct J 2022;119(1):131–43.
[22] Bugeja MN, Bracci JM, Moore WP. Seismic behavior of composite RCS frame systems. J Struct Eng ASCE 2000;126(4):429–36.
[23] ACI Committee 318. Building code requirements for structural concrete (ACI 318-19) and commentary (ACI 318R-19). American Concrete Institute, Farmington Hills, MI; 2019. p. 623.
[24] Ngo SH, Ou YC. Expected maximum moment of multi-spiral columns. Eng Struct 2021;249:113386. https://doi.org/10.1016/j.engstruct.2021.113386.
[25] Ngo SH, Ou YC, Nguyen VD. Shear strength model for reinforced concrete bridge columns with multispiral transverse reinforcement. J Struct Eng 2022;148(3). https://doi.org/10.1061/(ASCE)ST.1943-541X.0003289.
[26] Ou YC, Li JY, Roh H. Shear strength of reinforced concrete columns with five-spiral reinforcement. Eng Struct 2021;233:111929. https://doi.org/10.1016/j.engstruct.2021.111929.
[27] ABAQUS/CAE 2020 2019_09_14-01.49.31 163176. Dassault Systèmes Simulia Corp, Johnston, RI, USA.
[28] Behnam H, Kuang JS. Exterior RC wide beam–column connections: effect of spandrel beam on seismic behavior. J Struct Eng ASCE 2018;144(4):04018013. https://doi.org/10.1061/(ASCE)ST.1943-541X.0001995.
[29] Behnam H, Kuang JS, Huang RYC. Exterior RC wide beam-column connections: effect of beam width ratio on seismic behaviour. Eng Struct 2017;147:27–44.
[30] Yang H, Zhao W, Zhu Z, Fu J. Seismic behavior comparison of reinforced concrete interior beam-column joints based on different loading methods. Eng Struct 2018; 166:31–45.